The Journal of Engineering

The 9th International Conference on Power Electronics, Machines and Drives (PEMD 2018)

IET Journals
The Institution of Engineering and Technology

Modelling and control of the roll-stabilised control unit of a rotary steerable system directional drilling tool

eISSN 2051-3305
Received on 25th June 2018
Revised 03rd August 2018
Accepted on 09th August 2018
doi: 10.1049/joe.2018.8211
www.ietdl.org

Hamid Alterbeh[1] ✉, James F. Whidborne[2], Patrick Luk[2], Martin Bayliss[3]

[1]*University of Huddersfield, UK*
[2]*Cranfield University, UK*
[3]*Schlumberger, Stonehouse, UK*
✉ *E-mail: h.alturbeh@hud.ac.uk*

Abstract: A directional drilling tool control unit whose design is based on servo control of a rotary valve using the roll-stabilised instrumented system approach has been successfully used in oil fields for over 20 years. Here, field-oriented control (FOC) is applied to cascaded voltage regulation and servo control using an open-loop plant model of the roll-stabilised control unit. The servo control is applied to the rotary valve so that drilling mud is ported in a geostationary direction despite the rotation of the drill string and the bottom hole assembly of the rotary steerable system. Voltage regulation is applied in order to provide a DC voltage bus for the servo control of the valve. A torquer or alternator, which is a type of permanent magnet synchronous machine, is the core of the roll stabilised control unit. So, a mathematical model of the torquer is derived. An FOC scheme is proposed for servo control and to provide a DC regulated voltage using the torquers. The algorithm is tested in MATLAB/Simulink.

1 Introduction

For reference, Fig. 1 shows the main components of a typical roll stabilised system (RSS) directional drilling system incorporating a drilling tool whose control unit is the subject of this paper. In Fig. 1, it can be seen that the combination of the drill string and bottom hole assembly (BHA) can be viewed as a long flexible prop-shaft transmitting torque to the bit down-hole. In the annular clearance between the well bore and the drill string/BHA, mud returns to the surface as a means of lubrication and cuttings transport (amongst other functions) after being pumped from the surface through the centre of the drill string/BHA. The drill string/BHA is suspended from the block set weight on bit actuator at the drill rig on the surface, which is also where the top drive rotational actuator is situated.

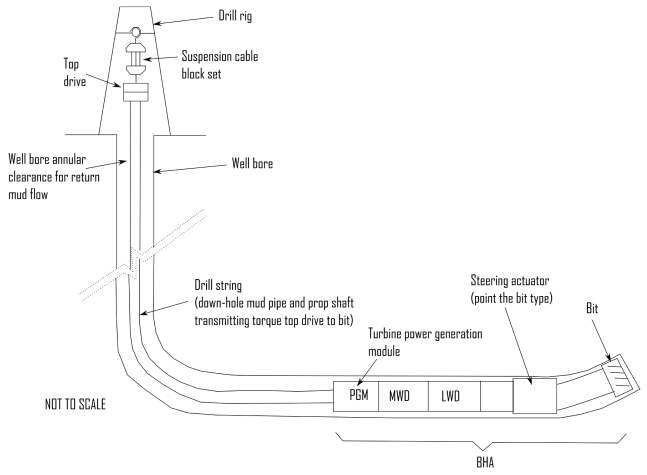

Fig. 1 *RSS directional drilling components [1]*

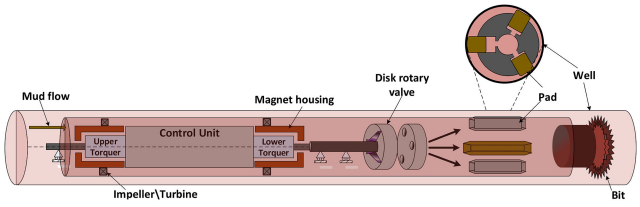

Fig. 2 *Roll-stabilised control unit*

The unique electro-mechanical architecture of the Schlumberger roll-stabilised control unit detailed here as part of the drilling system is shown schematically in Fig. 2. The rotary valve is mechanically continuous with the roll-stabilised platform, which is mounted on bearings so that it is able to rotate independently relative to the control unit collar (which spins with the BHA and drill string) about a common longitudinal axis. Two alternators/torquers are separately mounted on the roll-stabilised platform. Each torquer/alternator is of a permanent magnet synchronous motor (PMSM) type, but differs from a normal PMSM in that both parts (inner and outer) are free to rotate. A similar machine was presented in [2] to be used for hybrid vehicles as an integrated energy transducer. The control unit provides a regulated voltage power supply using energy extracted from the inner annular mud flow (between the collar and the control unit outside diameter) pumped from the surface using the torquer rotor-mounted impellers. This implies that the torquer stator (inner part) windings on the roll-stabilised platform are geostationary. Additionally, the geostationary roll-stabilised platform is required to be precisely servo-controlled relative to a geostationary position with respect to an external absolute reference by balancing the torque that acts on the common shaft.

2 Roll-Stabilised unit model

The torquers on the RSS are, in principle, normal PMSM alternators with the exception that the stator rotates. In a normal PMSM, the speed of the rotor is the only speed that needs to be considered for modelling the machine in the direct and quadrature (d, q) reference frame. In the RSS torquer case, the speed of the inner part (the stator) ω_s must be taken into consideration. Hence, instead of rotating the (d, q) reference frame at the speed of the rotor $\omega = \omega_r$, it rotates at the relative speed between the rotor and stator (i.e. $\omega = \omega_r - \omega_s$). Thus, the direct and quadrature voltage components in the (d, q) reference frame can be written as

$$u_d = R_s I_d + \frac{d\psi_d}{dt} - (\omega_r - \omega_s)\psi_q \tag{1}$$

$$u_q = R_s I_q + \frac{d\psi_q}{dt} + (\omega_r - \omega_s)\psi_d \tag{2}$$

where I_d and I_q are the direct and quadrature current components, respectively, R_s is the stator resistance and $\psi_d = L_d I_d + \psi_m$ and $\psi_q = L_q I_q$ are the direct and quadrature axis flux linkage components, respectively. The parameters L_d and L_q are the stator inductances for the direct and quadrature axes, respectively, and ψ_m is the constant flux produced by the permanent magnets. The electromagnetic torque is given by

$$T_e = \frac{3}{2}P[\psi_m I_q + (L_d - L_q)I_d I_q] \tag{3}$$

where P is the number of pole pairs. The mechanical governing equation is given by:

$$J\frac{d\omega}{dt} = T_e - b\omega - T_m \tag{4}$$

where J is the inertia, b is the fraction coefficient and T_m is the load torque. Thus, the mathematical model for the roll-stabilised control unit is given as follows:

$$\begin{bmatrix} \dot{i}_{d1} \\ \dot{i}_{d1} \\ \dot{\omega}_{r1} \\ \dot{i}_{d2} \\ \dot{i}_{q2} \\ \dot{\omega}_{r2} \\ \dot{\omega}_s \\ \dot{\theta}_s \end{bmatrix} = \begin{bmatrix} \frac{1}{L_d}[u_{d1} - R_s i_{d1} + (\omega_{r1} - \omega_s)L_q i_{q1}] \\ \frac{1}{L_q}[u_{q1} - R_s i_{q1} - (\omega_{r1} - \omega_s)(L_q i_{d1} + \psi_m)] \\ \frac{1}{J_{r1}}\left[\frac{3P}{2}\psi_m i_{q1} - T_{m1} - b\omega_{r1}\right] \\ \frac{1}{L_d}[u_{d2} - R_s i_{d2} + (\omega_{r2} - \omega_s)L_q i_{q2}] \\ \frac{1}{L_q}[u_{q2} - R_s i_{q2} - (\omega_{r2} - \omega_s)(L_q i_{d2} + \psi_m)] \\ \frac{1}{J_{r2}}\left[\frac{3P}{2}\psi_m i_{q2} - T_{m2} - b\omega_{r2}\right] \\ \omega_s \end{bmatrix} \tag{5}$$

where subscripts 1 and 2 refer to the upper and lower torquers, respectively, and subscripts r and s refer to the outer and inner parts of the torquer, respectively.

Using the FOC control scheme for the torquers, the speed and position of the inner part are servo-controlled, hence the rotary valve geostationary angle is maintained. In addition, with the assumption of FOC, one of the torquers can be controlled to provide a regulated supply voltage to the other servo-controlling torquer. The two control functions are uncoupled using bandwidth separation such that the speed of the voltage regulation is sufficiently fast in comparison with the servo control loop. The FOC technique makes designing the control for PMSM machines more straightforward since the q quadrature phase current can be made proportional to the torque in a similar way to the control of DC machines [3]. However, the mechanical and electrical coupling between the upper and lower torquers increases the complexity of the system, and with the need for more sensors to measure the speed and position of both the outer and inner parts of each torquer to apply FOC, more cost will be incurred. This problem can be overcome by using estimation techniques such as Kalman filtering [4], but for this paper the relevant sensors are assumed part of the system.

3 Drive architecture

The drive architecture for the two torquers is as shown in Fig. 3 and has a lot in common with the 'converter-fed synchronous machine drive' architecture discussed by [5]. The control topology

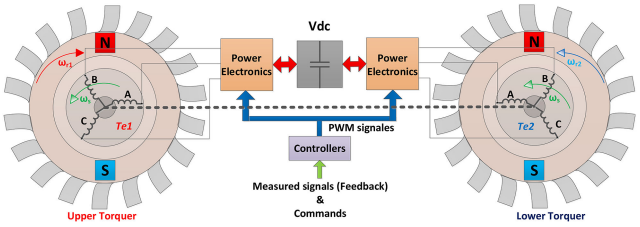

Fig. 3 *Drive architecture*

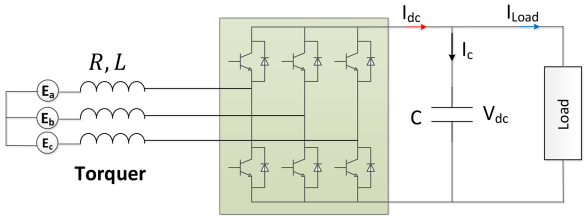

Fig. 4 *Power circuit of a PWM voltage-source converter*

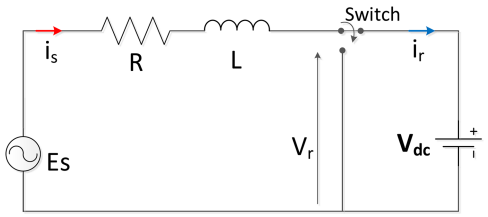

Fig. 5 *Per-phase equivalent circuit of a PWM VC converter*

is such that the upper torquer is controlled to provide voltage regulation of the voltage used by the motor control on the lower torquer. Therefore, the upper torquer is a regulated voltage source extracting energy from the mud flow using the torquer impeller. The lower torquer applies the servo control of the roll stabilised platform (the inner part common to both torquers) balancing the disturbance torques both from the mud impeller torque reactions and the electromagnetically induced torque balance between the two torquers.

3.1 Voltage regulation

The voltage regulation scheme is an extension of that given in [6] where feedback linearisation is used to provide a wider operating envelope than would otherwise be possible with a small perturbation-based linearisation control scheme. Feedback linearisation, as described by [7], is a technique where an inner loop linearises the input-state relationship and an outer loop stabilises the closed-loop dynamics. In this scheme, the upper torquer can be seen as rectifying the power taken from the mud as if it were a three-phase supply that connected to a PWM voltage-source converter as shown in Fig. 4. The power circuit of the PWM voltage-source converter that is shown in Fig. 4, where a resistive load is connected to the output terminal, can be represented by its per-phase equivalent circuit as shown in Fig. 5 (assuming $L_d = L_q = L$), where v_r is the converter input voltage.

The voltage equations in the (d, q) reference frame are:

$$E_d - u_d = R_s i_d + L\frac{di_d}{dt} - (\omega_r - \omega_s)Li_q \tag{6}$$

$$E_q - u_q = R_s i_q + L\frac{di_q}{dt} + (\omega_r - \omega_s)Li_d \tag{7}$$

The power balance between the AC and DC power gives:

$$\frac{3}{2}(E_d I_d + E_q I_q) = V_{\mathrm{dc}} I_d c \tag{8}$$

where the left-hand side represents the AC power and right hand side represents the DC power. The DC current I_{dc} is given by:

$$I_{\mathrm{dc}} = C\frac{dV_{\mathrm{dc}}}{dt} + I_L \tag{9}$$

where C is the capacity of the capacitor, and I_L is the load current. Substituting (9) in (8) and rearranging gives the state equation of the DC voltage as

$$\frac{dV_{\mathrm{dc}}}{dt} = \frac{3}{2CV_{\mathrm{dc}}}(E_d I_d + E_q I_q) - \frac{I_L}{C} \tag{10}$$

The non-linear governing equations representing the voltage regulator shown in Fig. 4 with the assumption that $\dot{\omega} = 0$ are:

$$\dot{x} = f(x) + gu, y = h(x) \tag{11}$$

$$\dot{x} = \begin{bmatrix} \dot{I}_d \\ \dot{I}_q \\ \dot{V}_{\mathrm{dc}} \end{bmatrix}, \quad y = \begin{bmatrix} I_d \\ V_{\mathrm{dc}} \end{bmatrix}, \quad u = \begin{bmatrix} u_d - 0 \\ u_q - E_q \end{bmatrix}$$

$$f(x) = \begin{bmatrix} f_1 \\ f_2 \\ f_3 \end{bmatrix} = \begin{bmatrix} -\frac{R_s}{L} I_d + \omega I_q \\ -\frac{R_s}{L} I_q - \omega I_d \\ \frac{3}{2CV_{\mathrm{dc}}} E_q I_q - \frac{I_L}{C} \end{bmatrix}, \quad g = \begin{bmatrix} \frac{1}{L} & 0 \\ 0 & \frac{1}{L} \\ 0 & 0 \end{bmatrix}$$

The control objectives are to regulate I_d at zero (as per FOC control practice) and V_{dc} at the required voltage DC-bus value using the FOC space vector modulated (SVM) voltage control inputs u_d and u_q. Differentiating the controlled outputs $y_1 = I_d$ and $y_2 = V_{\mathrm{dc}}$ until the inputs appear and re-arranging gives:

$$\begin{bmatrix} \dot{y}_1 \\ \ddot{y}_2 \end{bmatrix} = A(x) + E(x)\begin{bmatrix} u_1 \\ u_2 \end{bmatrix} \tag{12}$$

$$A(x) = \begin{bmatrix} f_1 \\ \frac{3}{2CV_dc} E_q f_2 - \frac{3f_3}{2CV_{\mathrm{dc}}^2} E_q I_q - \frac{I_L}{C} \end{bmatrix}$$

$$E(x) = \begin{bmatrix} \frac{1}{L} & 0 \\ 0 & \frac{3E_q}{2CV_{\mathrm{dc}}L} \end{bmatrix}$$

Therefore, the controller gains u_1 and u_2 can be evaluated:

$$\begin{bmatrix} u_1 \\ u_2 \end{bmatrix} = E^{-1}(x)\left[-A(x) + \begin{bmatrix} v_1 \\ v_2 \end{bmatrix}\right] \tag{13}$$

For tracking control, the new control inputs are given as

$$\begin{bmatrix} v_1 \\ v_2 \end{bmatrix} = \begin{bmatrix} \dot{y}_{1ref} - k_{11}e_1 - K_{12}\int e_1 dt \\ \ddot{y}_{2ref} - k_{21}\dot{e}_2 - k_{22}e_2 - k_{23}\int e_2 dt \end{bmatrix}. \tag{14}$$

where $e = y - y_{\mathrm{ref}}$ and $\dot{e} = \dot{y} - \dot{y}_{\mathrm{ref}}$. Thus, the output errors are given by:

$$\ddot{e}_1 + k_{11}\dot{e}_1 + k_{22}e_1 = 0 \tag{15}$$

$$\ddot{e}_2 + k_{21}\ddot{e}_2 + k_{22}\dot{e}_2 + k_{23}e_2 = 0 \tag{16}$$

The integral terms in (14) are added to eliminating any tracking errors that may occur due to parameter variation. The gains k_{ij} can be calculated by locating the desired poles on the left-half plane. Fig. 6 shows a schematic of the feedback linearisation controller generating the u_d and u_q FOC SVM inputs.

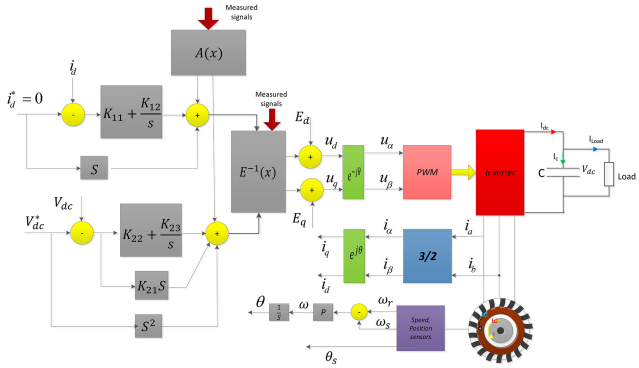

Fig. 6 *Feedback linearisation implementation*

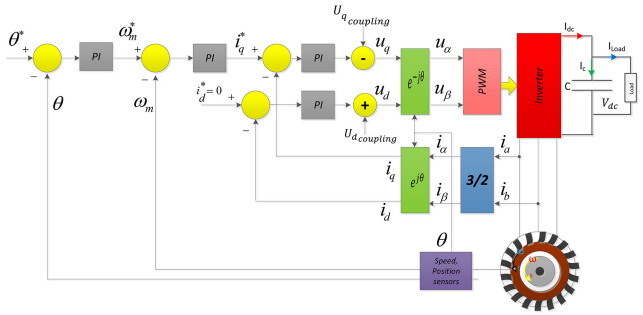

Fig. 7 *Servo control architecture*

3.2 Servo control

The servo control is implemented on the lower torquer and uses the standard architecture shown in Fig. 7. There are three cascaded control loops, the slowest outer position loop, the middle velocity loop with the inner current control loop taking its set-point current demand from the velocity loop and using FOC to work in the (d, q) reference frame.

As FOC is used, the open-loop plant for the inner current control loop is of the form $((1/L)/s + R/L)$, hence a nested PI-SISO architecture is used with pole placement gains given by $L\omega_n^2$ and $2L\delta\omega_n - R$ for the forward-path integral and the feedback path proportional gains, respectively. The closed-loop control specification are the natural frequency ω_n and the damping ratio δ.

The middle velocity loop is proportional only and can be designed using pole placement assuming a first-order lag open loop plant. The assumption that the open loop plant in first order is reasonable given its dominant dynamics will be an inertia and friction dominated second order transfer function the derivative of which will be a first order lag. Hence, it can be deduced that the pole placement proportional gain is given by $(J_s - C_s\tau_1)/\tau$ where τ_1 is the control specification for the velocity response time constant.

Finally, the plant for the outer position loop can be taken as a pure integrator given the assumption that the velocity loop is sufficiently fast. Therefore, a nested PI-SISO architecture is used for the position loop with pole placement gains given by ω_n^2 and $2\delta\omega_n$ for the forward path integral and the feedback path proportional gains, respectively.

4 Simulation

A transient simulation of the system was created in MATLAB/ Simulink using the parameters stated in Table 1. The simulation consisted of the non-linear open-loop plant and the voltage regulating and servo controllers. The electro-magnetic part of the open-loop plant was expressed in the (d, q) reference frame and coupled to the rotational mechanical dynamics as per the governing (5). The control specification for the voltage regulating and servo control loops are as shown in Table 2.

Table 1 Transient simulation parameters

Parameter	Description	Value
L_q, L_d	(d, q) phase inductance	8.5 mH
R_s	(d, q) phase stator resistance	2.875 Ω
C	voltage regulator shunt cap.	660 mF
ψ_m	flux linkage	01.75 V s rad^{-1}
P	number of pole pairs	4
J_s	inner part inertia	6.0×10^{-3} kg m^2
J_r	outer part inertia	0.1×10^{-3} kg m^2

Table 2 pole placement control specifications

Symbol	Loop & description	Value
δ	all loops closed loop damping ratio	0.707
ω_{n1}	position, natural frequency	1.257 rad s^{-1}
τ_1	velocity, time constant	1 ms
ω_{n2}	current, natural frequency	25.13 rad s^{-1}
ω_{n3}	voltage, first natural frequency	100.0 rad s^{-1}
ω_{n4}	voltage, second natural frequency	50.0 rad s^{-1}
τ_2	voltage, pole time constant	0.20 s

4.1 Simulation results: command signal tracking

Fig. 8 shows the geostationary position response of the servo-controlled inner part, regulated DC voltage, and the load current. It can be seen that the geostationary position (inner control loop) tracks the demand positions of 90° and step change of 180° at 5 s with zero steady-state error with fast response times and small overshoots. The inner part position also tracks a ramp change of reference position from 180° to 0° starts at 8 s with slope of 10 rad/s. The regulated voltage V_{dc} shown in Fig. 8 has a zero steady-state error 100 V response and rapid transient response (relative to the inner part position response) when a step change of 110 V is applied at 10 s with good disturbance rejection of the resistance load step change at 12 s and corresponding load current I_L drop. It can be seen that the magnitude of the regulated voltage disturbance, which is related to the position disturbance, is very small when the position disturbance is a ramp signal. However, the regulated voltage disturbance reaches about 15% when the position demand is a step signal. At 12 s, the small disturbance is due to a step change in the load resistance R_L from 25 to 50 Ω.

Fig. 9 shows the upper and lower impeller speeds ω_{r1} and ω_{r2} which have very fast response times (low inertia) and are nominally equal and opposite in magnitude. Also shown on Fig. 9 is the regulating action of the middle velocity loop with the steady-state speed being zero apart from the brief transients due to position and load resistance step changes at 5, 8, and 12 s. Fig. 10 shows the control outputs from the FOC to the SVM showing response due to the position and load resistance step changes.

4.2 Simulation results: effects of the disturbances on the system responses

The operation of the roll stabilised unit depends on the torques T_{m1} and T_{m2} that rotate the outer parts of the upper and lower torquers, respectively. These torques are generated by the mud flow that is pumped from the surface. The mud flow is not constant and can change for many reasons. For example, in down-hole drilling scenario mud-pulse telemetry is used to communicate with down-hole computers via downlinks by encoding a rectangular pulse train on top of the normal drilling fluid/mud flow. This creates a time varying flow rate as it decreases the magnitude of the mud flow by 5–25% [8]. Another disturbance results from the torque T_s which acts on the inner part of the torquer. The T_s torque is also time varying which may increase or decrease during the operation. Thus, testing the proposed control strategies in the presence of

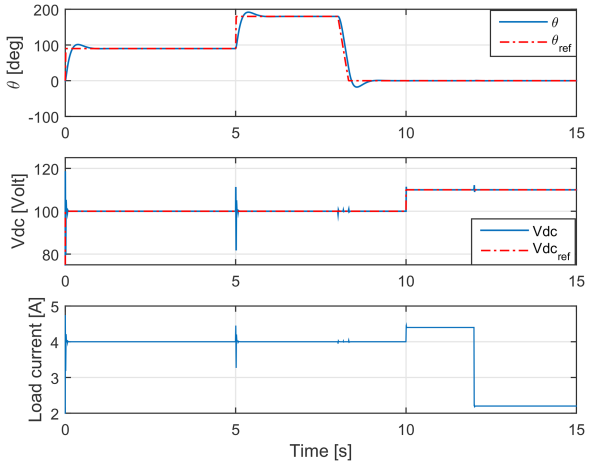

Fig. 8 *Inner part position response θ, regulated voltage V_{dc}, and load current I_L*

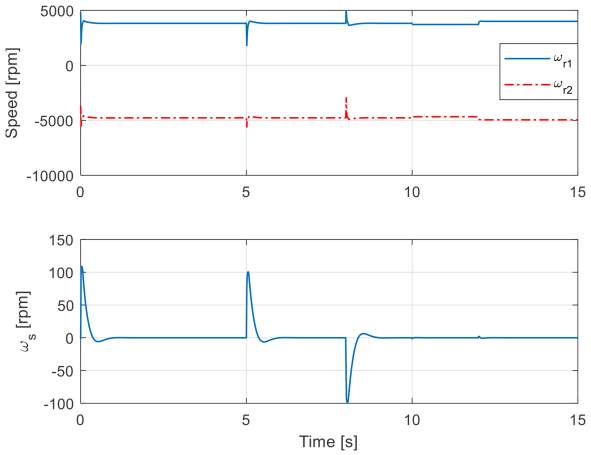

Fig. 9 *Impeller and geostationary inner part speed responses*

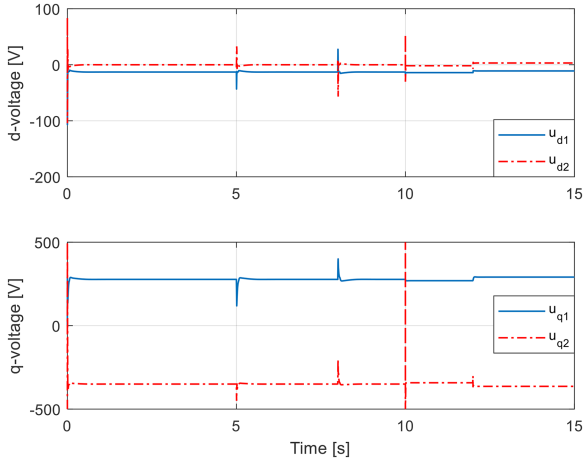

Fig. 10 *Regulator (u_{d1}, u_{q1}) and servo control (u_{d2}, u_{q2}) voltages*

these disturbances is important to show the robustness of the controllers against the external disturbances.

Fig. 11 shows the disturbance torques that are applied to the roll stabilised control unit and the responses of the inner part position, θ, and the DCc voltage, V_{dc}, during 10 s of simulation. The disturbances and the input signals are defined as the following

- The torque disturbance on the inner part is $T_s = 0$ Nm for $2 > t > 6$ s, $T_s = 3.0$ Nm for $2 \geq t \leq 4$ s, and $T_s = -3.0$ Nm for $4 \geq t \leq 6$ s.

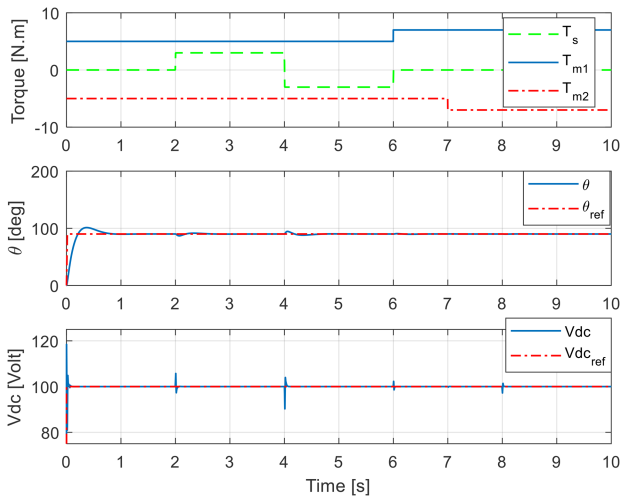

Fig. 11 *Disturbances and controlled outputs*

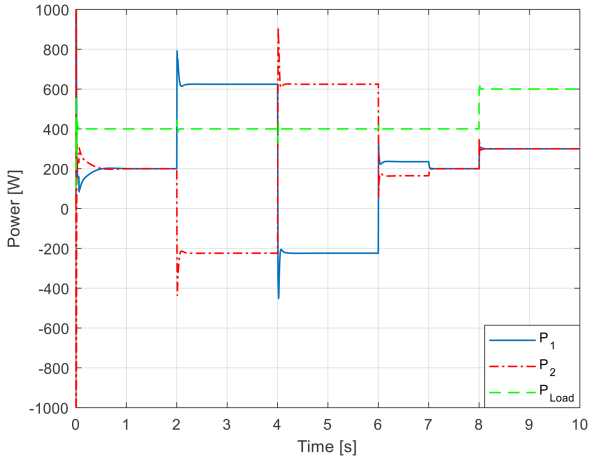

Fig. 12 *Generated/consumed power of the upper torquer, the lower torquers, and the load*

- The input mud flow torque that acts on the upper torquer's impeller is $T_{m1} = 5.0\,\text{Nm}$ for $t < 6\,\text{s}$, and $T_{m1} = 7.0\,\text{Nm}$ for $t \geq 6\,\text{s}$.
- The input mud flow torque that acts on the lower torquer's impeller is $T_{m2} = -5.0\,\text{N m}$ for $t < 7\,\text{s}$, and $T_{m2} = -7.0\,\text{Nm}$ for $t \geq 7\,\text{s}$. The negative value of T_{m2} is because the lower torquer rotates the opposite direction to the upper torquer.
- The load value, which is modelled as a resistance, is decreased at 8 s from $R = 25.0\,\Omega$ to $R = 12.5\,\Omega$.
- The tool face (position) is $\theta = 0°$ for $t < 0\,\text{s}$, and $\theta = 90°$ for $t \geq 0\,\text{s}$.
- The regulated dc voltage is $V_{\text{dc}} = 0\,\text{V}$ for $t < 0\,\text{s}$, and $V_{\text{dc}} = 100\,\text{V}$ for $t \geq 0\,\text{s}$.

It can be seen in Fig. 11 that the servo controller maintains the position of the inner part at the reference value ($\theta = 90°$) and overcomes the T_s disturbances at 2 and 4 s with <1 s for the recovery. However, the effect of the disturbances of the T_{m1}, T_{m2}, and the load is small enough to be neglected. The DC voltage response is disturbed by T_s, T_{m1}, T_{m2}, and the load. Additionally, it can be observed that the larger the disturbance in T_s, the greater the effect on the V_{dc}. For example, V_{dc} is disturbed by ∼10% at 4 s when T_c goes from 0 to 3 Nm which is twice that at 2 s when T_c is changed from 3 to −3 Nm. For this scenario, V_{dc} is less affected by the changes on T_{m1}, T_{m2}, and the load than the changes on T_s. However, the recovery time in all cases is very small (less than 0.1 s) which is much smaller than the recovery time of the position.

Note that the assumed scenario is a very extreme case where the disturbances are introduced as step signals, which may be realistic for the load (as load resistance can be changed suddenly due to a short circuit or disconnection), but is unusual for the mechanical torques that are acting on the inner or outer part of the torquers. In practice, these torques change gradually.

Fig. 12 shows the power of the upper torquer P_1, lower torquer P_2, and the load P_L. For the torquer, positive power means that the torquer is operating in generating mode, while negative power means motoring mode. The load is always consuming power. It can be seen in Fig. 12 that both torquers are generating power between 0 and 2 s, but when a disturbance on T_s is introduced, the upper torquer keeps generating power at a higher rate but the lower torquer starts motoring. When the T_s disturbance is reversed from 3 to −3 Nm at 4 s, the operating modes of the torquers are reversed (i.e. the upper torquer becomes a motor and the lower torquer becomes a generator). When T_s disturbance is removed at 6 s (i.e. $T_s = 0\,\text{Nm}$), both torquers return to operate in the generating mode. When both torquers are operating in generating mode, the generated power is consumed by the load. However, in the cases when just one torquer is generating and the other is motoring, the generated power is consumed by the load and the motor. So the summation of the power that is generated/consumed by the torquers are always equal to the load power.

5 Conclusion

This paper details the design of a cascaded control system for voltage regulation and servo control of a roll stabilised control unit typically used for RSS directional drilling in the oil and gas industry. The electromechanically coupled open loop plant is derived in the FOC (d, q) reference frame and then feedback linearisation and standard servo design techniques are applied for the bandwidth separated voltage regulation and servo controllers, respectively.

6 Acknowledgments

This research was funded by Schlumberger. The proposed system is patented (application) in the United State (US Patent US20170067332).

7 References

[1] Panchal, N., Bayliss, M.T., Whidborne, J.F.: 'Attitude control system for directional drilling bottom hole assemblies', *IET Control Theory Appl.*, 2012, **6**, (8), pp. 884–892

[2] Backstrom, T., Sadarangani, C., Ostlund, S.: 'Integrated energy transducer for hybrid electric vehicles'. Eighth Int. Conf. on Electrical Machines and Drives (IEE Conf. Publ. No. 444), Cambridge, UK, September 1997, pp. 239–243

[3] Blaschke, F.: 'The principles of field orientation as applied to the new TRANSVEKTOR closed-loop control system for rotating field machines', *Siemens Rev.*, 1972, **34**, pp. 217–220

[4] Vas, P.: '*Sensorless vector and direct torque control*' (Oxford University Press, Oxford UK, 1998)

[5] Hughes, A., Drury, B.: '*Electric motors and drives: fundamentals, types and applications*' (Newnes, Oxford, UK, 2013, 4th edn.)

[6] Lee, D., Lee, G., Lee, K.-D.: 'DC-bus voltage control of three-phase AC/DC PWM converters using feedback linearization', *IEEE Trans. Ind. Appl.*, 2000, **36**, (3), pp. 826–833

[7] Slotine, J., Li, W.: '*Applied nonlinear control*' (Prentice Hall, Englewood Cliffs, NJ, 1991)

[8] Johnson, T.T., Hoefel, A.E.: 'Turbo-alternator stalling protection using available-power estimate'. Power and Energy Conf. at Illinois (PECI), Champaign, IL, USA, 2011

2019-04-26

Modelling and control of the roll-stabilised control unit of a rotary steerable system directional drilling tool

Alturbeh, Hamid

IET

Alterbeh H, Whidborne JF, Luk P, Bayliss M. (2019) Modelling and control of the roll-stabilised control unit of a rotary steerable system directional drilling tool. Journal of Engineering, Volume 2019, Issue 17, June 2019, pp. 4555-4559

https://doi.org/10.1049/joe.2018.8211